Analysis of an Infinite Phased Array of Aperture Coupled Microstrip Patches

DAVID M. POZAR, SENIOR MEMBER, IEEE

Abstract—**An analysis of an infinite array of aperture coupled microstrip patch antennas is described; this type of element is well suited to integrated phased array applications, offering several advantages over other array configurations. The solution employs the spectral domain moment method approach, and combines features of a previous solution for infinite arrays of probe-fed patches and a reciprocity analysis of a single aperture coupled microstrip element. The theoretical analysis is described and data are presented for the active input impedance of several arrays. Experimental data from a waveguide simulator confirm the theory.**

I. Introduction

THE GEOMETRY of an aperture coupled microstrip antenna [1] is shown in Fig. 1. It consists of two substrates bonded together, with a ground plane in between. The radiating patch is printed on the top (antenna) substrate, while a microstrip feedline is printed on the bottom (feed) substrate. A small nonresonant aperture in the ground plane couples the patch to the feedline. This aperture radiates some power below the ground plane, but because the aperture is below resonant size, this power is typically 20 dB or more below the patch power level [1]. The bandwidth is essentially that of the patch antenna itself, and is not affected by the aperture coupling mechanism. The aperture coupled microstrip antenna was originally developed as a candidate element for integrated phased array antennas, and has the following attractive features [1]–[3]:

- Substrate real estate is available on both sides of the array for radiating elements, feed networks, phase shifters, bias and control lines, and other active circuitry.
- The substrates can be matched to the two distinct electrical functions of radiation (electrically thick, low ϵ_r), and circuitry (electrically thin, high ϵ_r).
- The scan blindness-bandwidth trade-off [2] is improved since a low ϵ_r substrate can be used for the radiating elements.
- No direct contact to the radiating elements through the substrate (via holes or coaxial probes) is required, enhancing manufacturability and reliability.

The single aperture coupled patch antenna has been theoretically analyzed in [4], [5], and a similar analysis has been reported for an aperture coupled dipole [6]. Useful design data concerning the effect of aperture size and position, and tuning stub length, is given in [4]. Since the aperture coupled microstrip element is intended for use in a large array configuration, the present paper addresses the problem of an infinite scanning array of aperture coupled patches. The analysis uses the exact Green's functions for the dielectric substrates in a spectral domain moment method solution, and is an extension of the solutions of [7] and [8], for printed dipoles and probe-fed microstrip patches. It is interesting to note that the aperture coupled patch array geometry is considerably more complicated than the probe-fed patch array of [8], but because the aperture feed does not involve a direct contact with the patch, it is easier to obtain a more rigorous solution for this case. Thus, the present solution accurately models the aperture coupling, and completely accounts for surface wave effects on both substrates and mutual coupling between all patches and coupling slots. Unlike the analysis of the idealized-probe-fed patch array in [8], the present solution is not limited to thin substrates.

Since the original aperture coupled patch design was reported [1], several variations of the basic geometry have been developed [9]–[12]. Although the geometries and me-

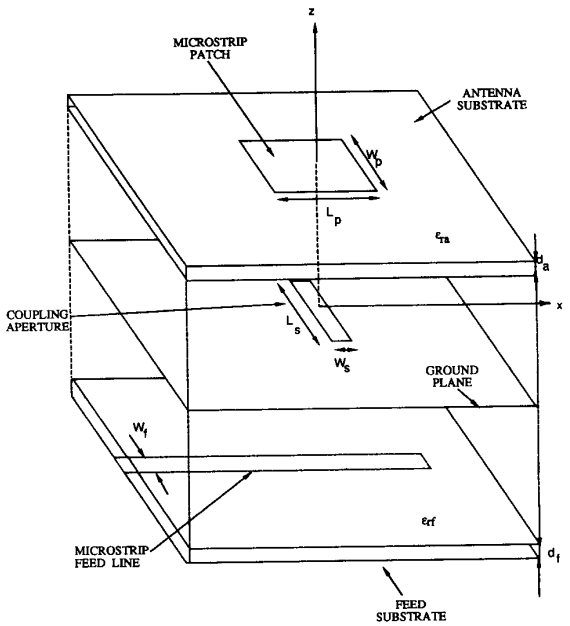

Fig. 1. Geometry of an aperture coupled microstrip patch antenna.

Manuscript received August 24, 1987; revised July 14, 1988. This work was supported by the National Science Foundation under Presidential Young Investigator Grant ECS 8352325, and by the Hughes Aircraft Corporation.

The author is with the Department of Electrical and Computer Engineering, University of Massachusetts, Amherst, MA 01003.

IEEE Log Number 8825317.

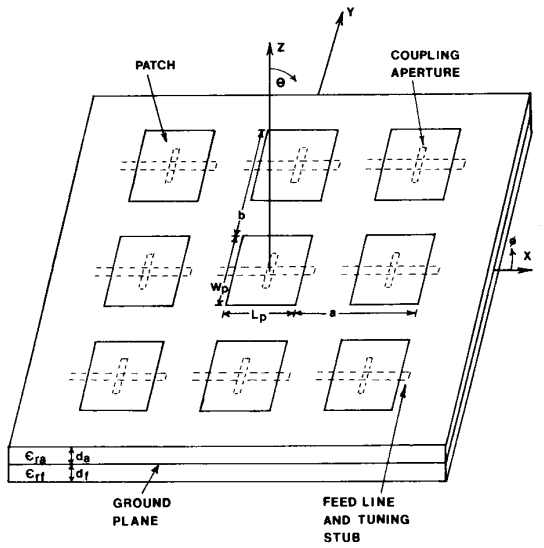

Fig. 2. Geometry of an infinite array of aperture coupled microstrip patches.

chanical features of these configurations may differ from the present case, it is felt that the electrical performance of arrays of such elements should be qualitatively similar to that reported here.

The following section describes the theory of the solution for the active input impedance of the infinite aperture coupled patch array. Section III then presents several theoretical results, and takes particular notice of the scan blindness effect and the fact that such blindnesses can occur due to forced surface wave resonances on *either* the antenna substrate or the feed substrate. This section also shows the results from a waveguide simulator experiment, which serves to validate the theory.

II. Theoretical Analysis

The analysis of the infinite array of aperture coupled patches combines the solution of [8] for an infinite array of probe-fed patches with that of [5] for a single aperture coupled patch element. The geometry of the array is shown in Fig. 2. Because of the periodicity of the array, all currents and fields must vary across the plane of the array as

$$e^{-jk_0(mau+nbv)}, \tag{1}$$

where

$$u=\sin\theta\cos\phi \tag{2a}$$

$$v=\sin\theta\sin\phi \tag{2b}$$

are the direction cosines of the scanned beam, and θ, ϕ is the scan angle.

The solution proceeds by replacing the apertures with oppositely directed equivalent magnetic currents on both sides of the ground plane, phased according to (1). The patch currents are then found as solutions to the electric field integral equation, with the slot currents as the excitation. It remains to couple the slots to the microstrip feedlines, which is done using the reciprocity technique of [5]. At this point it is assumed that the feedlines for the elements do not interact (no mutual coupling between the feedlines themselves), which is a quite reasonable assumption for a practical microstrip circuit. For purposes of analysis, then, the coupling of one aperture in the infinite array to its associated feedline is found, and an equivalent series impedance is determined. This impedance represents the active impedance of the array seen by any of the microstrip feedlines; once this quantity is determined, microwave circuit theory can be used to find the active input impedance of the (typically) stub-tuned array elements. In this way, the feedlines can be routed in any desired fashion on the feed substrate, as long as they do not come within a few substrate thicknesses of each other.

Because the coupling apertures are electrically small (on the order of $\lambda_0/10$), the aperture electric field can be approximated with a single piecewise-sinusoidal (PWS) expansion mode:

$$e_x^a(x, y)=f_u(x, W_s)f_p(y, L_s/2) \tag{3}$$

where f_u is a uniform distribution and f_p is a PWS distribution, as defined in the Appendix. In (3), the field is written for the unit cell centered at $x = y = 0$; it is assumed that other unit cells have the same aperture distribution, but phased according to (1). It is also assumed that the aperture is centered below the patch, which is usually true in practice, since the tightest coupling then results.

We now use entire domain modes to expand the patch currents. For $\hat{x}$-directed surface currents, the ith expansion mode is

$$\bar{J}_i(x, y)=\hat{x}f_s(x, k, L)f_c(y, l, W), \tag{4a}$$

while for $\hat{y}$-directed surface currents the ith expansion mode is

$$\bar{J}_i(x, y)=\hat{y}f_c(x, k, L)f_s(y, l, W), \tag{4b}$$

where k, l are integer indices accounting for the number of variations in the x and y directions, respectively, for the ith expansion mode.

Then the electric field integral equation can be used to enforce the boundary condition that the total E_x and E_y fields (due to the slot excitation and the currents excited on the patch) are zero over the patch surface. This results in the matrix equation

$$[Z][I]=[V^M], \tag{5}$$

where $[I]$ is the column vector of unknown patch expansion mode coefficients, $[Z]$ is the moment method impedance matrix of the patch, and $[V^M]$ is the voltage vector due to the excitation of the magnetic currents in the apertures. From [8], the elements of the impedance matrix are given by

$$Z_{ij}=-\int_{S_i}\bar{J}_i(x, y)\cdot\bar{E}_j(x, y)\,ds_i$$

$$=\frac{-1}{ab}\sum_{m=-\infty}^{\infty}\sum_{n=-\infty}^{\infty}\bar{F}_i(k_x, k_y)$$

$$\cdot\bar{\bar{G}}^{EJ}(k_x, k_y)\cdot\bar{F}_j^*(k_x, k_y), \tag{6}$$

where $\bar{E}_j$ is the electric field due to the jth expansion mode, $\bar{F}_i$ is the Fourier transform of the ith expansion/test mode as defined in the Appendix, and

$$\bar{\bar{G}}^{EJ} = \hat{x}G_{xx}^{EJ}\hat{x} + \hat{x}G_{xy}^{EJ}\hat{y} + \hat{y}G_{yx}^{EJ}\hat{x} + \hat{y}G_{yy}^{EJ}\hat{y}, \tag{7}$$

is a spectral domain Green's function dyadic [8] representing the transverse electric field from a transverse electric dipole. Thus, G_{pq}^{EJ} represents the $\hat{p}$-component of the electric field due to a $\hat{q}$-directed electric source, in the spectral domain. Expressions for these components are given in the Appendix. In (6), as well as forthcoming expressions, the variables k_x and k_y take on the following discrete values:

$$k_x = \left(\frac{2\pi m}{a} + k_0 u\right), \tag{8a}$$

$$k_y = \left(\frac{2\pi n}{b} + k_0 v\right). \tag{8b}$$

From [5], the elements of the voltage vector are given by

$$V_i^M = \int_s \bar{J}_i(x, y) \cdot \bar{E}^{\text{inc}}(x, y)\, ds$$

$$= \frac{1}{ab} \sum_{m=-\infty}^{\infty} \sum_{n=-\infty}^{\infty} \bar{F}_i(k_x, k_y) \cdot \bar{G}_y^{EM}(k_x, k_y) F_u^*(k_x) F_p^*(k_y), \tag{9}$$

where $\bar{E}^{\text{inc}}$ is the incident field caused by the aperture magnetic current e_x^a, and

$$\bar{G}_y^{EM} = \hat{x}G_{xy}^{EM} + \hat{y}G_{yy}^{EM}, \tag{10}$$

is a spectral domain Green's function representing the $\hat{x}$ or $\hat{y}$ electric field due to a $\hat{y}$-directed infinitesimal magnetic current; the necessary components are listed in the Appendix. F_u and F_p are Fourier transforms of the aperture fields of (3), and are also given in the Appendix.

Now an aperture admittance $Y^S + Y^P$ can be defined as the reaction of the aperture electric field and the sum of the direct magnetic field from the slot (Y^S) and the scattered field from the patch (Y^P). The self-admittance of the slot is [5]

$$Y^S = Y^{S(a)} + Y^{S(f)} = \int_{S_a} e_x^a(x, y) H_y^M\, dS_a$$

$$= \frac{1}{ab} \sum_{m=-\infty}^{\infty} \sum_{n=-\infty}^{\infty} F_u^2(k_x) F_p^2(k_y) \cdot [G_{yy}^{HM(a)}(k_x, k_y) + G_{yy}^{HM(f)}(k_x, k_y)], \tag{11}$$

where H_y^m is the magnetic field radiated by the aperture, and $G_{yy}^{HM(a,f)}$ is the spectral domain Green's function representing the H_y field radiated on either the antenna (a) side or the feed (f) side of the ground plane, due to a $\hat{y}$-directed magnetic aperture current. These two terms are similar in form, but may have different values if different substrates are used on the two sides of the ground plane. The expression for G_{yy}^{HM} is given in the Appendix.

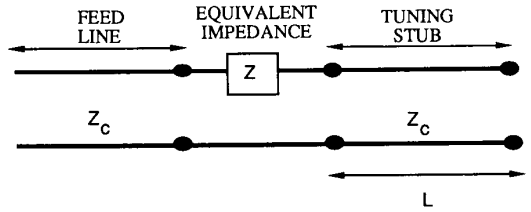

Fig. 3. Equivalent circuit of any given element of an infinite array of stub-tuned aperture coupled patches.

The contribution to the aperture admittance due to the scattered field of the patch is given by [5]

$$Y^P = \int_{S_a} e_x^a(x, y) H_y(x, y)\, dS_a = [V^J]^t [I], \tag{12}$$

where H_y is the magnetic field at the aperture due to the currents on the patch. The elements of the voltage vector $[V^J]$ are given as

$$V_i^J = \int_{S_a} e_x^a(x, y) H_{y_i}(x, y)\, dS_a = \frac{1}{ab} \sum_{m=-\infty}^{\infty} \sum_{n=-\infty}^{\infty} F_p(k_y) F_u(k_x) \cdot \bar{G}_y^{HJ}(k_x, k_y) \cdot \bar{F}_i^*(k_x, k_y), \tag{13}$$

where

$$\bar{G}_y^{HJ} = G_{yx}^{HJ}\hat{x} + G_{yy}^{HJ}\hat{y} \tag{14}$$

is a spectral domain Green's function representing the H_y field due to an $\hat{x}$ or $\hat{y}$-directed infinitesimal electric dipole; the individual components are listed in the Appendix.

Then, as derived in [5], the aperture coupled patches appear to the microstrip feed lines as series impedances Z, where Z is given by

$$Z = Z_c \frac{\Delta v^2}{Y^S + Y^P}, \tag{15}$$

where Z_c is the characteristic impedance of the feedline, and Δv is a modal voltage due to the discontinuity of the slot. From [5], Δv is given by

$$\Delta v = \int_{S_a} e_x^a(x, y) h_y(x, y)\, dS_a, \tag{16}$$

where $h_y(x, y)$ is the normalized magnetic field of the quasi-transverse electromagnetic (TEM) microstrip line mode [5]:

$$h_y(x, y) = \frac{1}{2\pi\sqrt{Z_c}} \int_{-\infty}^{\infty} F_u(k_y) G_{yx}^{HJ}(k_x = -\beta_m, k_y) \cdot e^{-j\beta_m x} e^{jk_y y}\, dk_y, \tag{17}$$

where β_m is the propagation constant of the microstripline.

Thus, the equivalent circuit of any given element of an infinite array of stub-tuned aperture coupled patches is as shown in Fig. 3. The equivalent impedance Z is found from

the above analysis, and the tuning stub can easily be treated using transmission line theory. If $Z_{in}(\theta, \phi)$ is the input impedance at a given point on the feedline (a phase reference at the aperture is used in this paper), for the scan angle θ, ϕ, then an active reflection coefficient can be defined as

$$R(\theta, \phi) = \frac{Z_{in}(\theta, \phi) - Z_{in}(0, 0)}{Z_{in}(\theta, \phi) + Z_{in}^{*}(0, 0)}, \tag{18}$$

thus ensuring that the array is matched at broadside. To be matched to the feedline at broadside, we should have $Z_{in}(0, 0) = Z_c$.

III. Results and Discussion

The above theory was implemented in a computer code for calculating the active input impedance of infinite arrays of aperture coupled patches. Consideration was given to computational efficiency by evaluating the Green's functions only once for a given set of k_x, k_y values, and calculating all of the impedance matrix elements (6) at the same time. It was found that 121 ($-60 \le m, n \le 60$) Floquet modes in each direction were enough to yield convergence of expressions (6), (9), (11), and (13). The evaluation of Δv in (15), (16) involves only a one-dimensional numerical integration, and is relatively fast. Total computation time, using five expansion modes on the patch, is about two minutes per scan angle on a MicroVAX II computer.

Fig. 5 shows the reflection coefficient magnitude versus scan angle for an infinite patch array with an antenna substrate having $\epsilon_{ra} = 2.55$, $d_a = 0.02\ \lambda_0$, and a feed substrate having $\epsilon_{rf} = 12.8$, $d_f = 0.05\ \lambda_0$. In practice, such a thick feed substrate would be undesirable, but has been used here to clearly illustrate the scan blindness effect for this type of array. The calculations were made with five expansion modes on the patch: three $\hat{x}$-directed currents with $(k, l) = (1, 0), (3, 0), (5, 0)$, and two $\hat{y}$-directed currents with $(k, l) = (0, 1), (0, 2)$. As expected from the cavity model of an isolated patch, the (1, 0) mode is the most important. The $\hat{y}$-directed modes had little effect except for D-plane ($\phi = 45°$) scanning. Other higher order modes were found to have negligible effect.

The array was matched to the 50 Ω microstrip feedline at broadside scan by adjusting the size of the aperture. As discussed in [10], the length of the aperture (L_s) controls the amount of coupling between the patch and the feedline; it is generally desired to make the aperture just long enough to achieve critical coupling. The length of the tuning stub (L) does not affect the level of coupling, but can be used to provide a reactive shift to rotate the impedance locus along constant resistance circles on the Smith chart.

The data of Fig. 4 are qualitatively similar to that of other printed phased arrays [7], [8]. As the array is scanned off broadside, impedance mismatch occurs in all scan planes. Of particular note, however, are the unity reflection coefficient magnitudes in the E-plane at $\theta = 62.7°$ and $\theta = 85.6°$. These scan blindnesses result from the forced resonance of surface waves on the feed and antenna substrates, respectively. This phenomenon has been observed for other printed phased arrays [7], [8], [13], and can be predicted by equating the

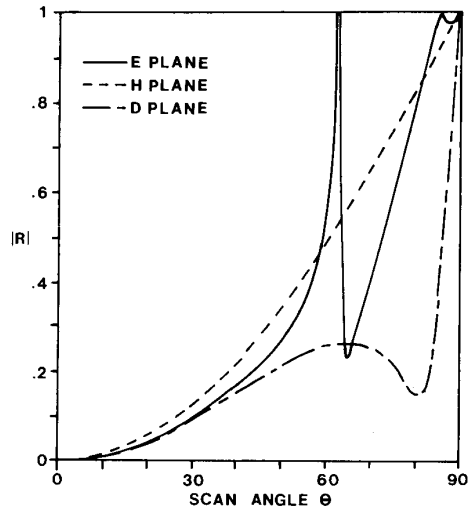

Fig. 4. Reflection coefficient magnitude versus scan angle for an infinite array of aperture coupled patches. $\epsilon_{ra} = 2.55$, $d_a = 0.02\ \lambda_0$, $\epsilon_{rf} = 12.8$, $d_f = 0.05\ \lambda_0$, $L_p = W_p = 0.29\ \lambda_0$, $L_s = 0.115\ \lambda_0$, $W_s = 0.01\ \lambda_0$, $W_f = 0.05\ \lambda_0$, $L = 0.075\ \lambda_0$, $a = b = 0.5\ \lambda_0$.

propagation constant β_{sw} of the first TM surface wave of the grounded dielectric substrate and the m, nth Floquet mode. Thus, when the following equation is satisfied for a given scan angle and Floquet mode,

$$(\beta_{sw}/k_0)^2 = (k_x/k_0)^2 + (k_y/k_0)^2 = \left(\frac{m}{a/\lambda_0} + u\right)^2 + \left(\frac{n}{b/\lambda_0} + v\right)^2, \tag{19}$$

all power is trapped in a surface wave-like field near the face of the array, and no real power is radiated. In practice, this effect usually occurs for the $m = -1$, $n = 0$ Floquet mode, but other solutions are possible [7]; as discussed in [7], a surface wave circle diagram, embodying (19), offers a convenient graphical technique for visualizing the scan blindness phenomenon and the effect of element spacings and substrate parameters (which affect β_{sw}).

Since there are two distinct substrates (separated by a ground plane) in the array of aperture coupled patches, two (or more) distinct scan blindnesses can occur. Thus, the blindness at $\theta = 62.7°$ in the data of Fig. 4 is due to surface wave resonance on the feed substrate (excited by the apertures), for which $\beta_{sw} = 1.11081 k_0$, while the blindness at $\theta = 85.6°$ is due to surface wave resonance on the antenna substrate (excited by the patches and the apertures), for which $\beta_{sw} = 1.00294 k_0$.

To study this effect more closely, we have plotted in Fig. 5 the real and imaginary parts of the admittances $Y^{S(a)}$, $Y^{S(f)}$, and Y^{P}, as given by (11) and (12), versus scan angle for E-plane scan. Fig. 5(a) shows that $\mathrm{Re}(Y^{P})$ approaches zero at $\theta = 85.6°$, the location of the blindness due to the antenna substrate, while $\mathrm{Re}(Y^{S(a)})$ or $\mathrm{Re}(Y^{S(f)})$ remain finite and nonzero. The $\mathrm{Re}(Y^{P})$ also shows a large peak just before $\theta = 85.6°$; this may be what has been referred to in [13] as a "leaky wave" resonance. It does not lead to a scan blindness, but it may result in a large mismatch. Fig. 5(b) shows the

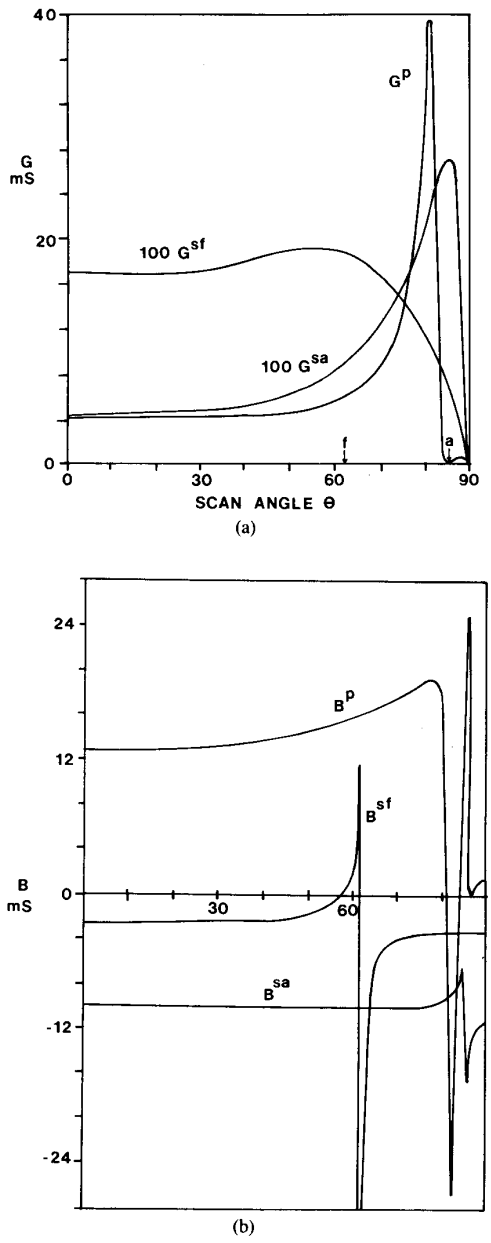

Fig. 5. (a) Real. (b) imaginary parts of $Y^{S(a)}$, $Y^{S(f)}$, and Y^P admittances versus E-plane scan angle for the geometry of Fig. 4.

imaginary parts of the admittances, where it is seen that $I_m(Y^{S(a)})$ and $I_m(Y^{S(f)})$ have very narrow singularities at $\theta = 85.6°$ and $\theta = 62.7°$, respectively; this behavior leads to scan blindness at those angles. In addition, $I_m(Y^P)$ goes through a resonance (associated with the leaky wave) just before $\theta = 85.6°$. This data shows that the patches are essentially open-circuited ($Y^P \simeq 0$) at the antenna substrate blindness at $\theta = 85.6°$; this may explain why the surface wave propagation constant of the *unloaded* dielectric slab can be used to accurately predict the scan blindness angle. Another interesting feature of the data of Fig. 4 is that this array does not show any blindness in the H-plane.

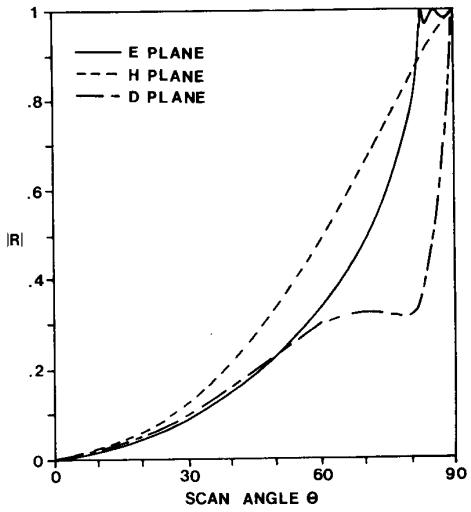

Fig. 6. Reflection coefficient magnitude versus scan angle for an infinite array of aperture coupled patches. $\epsilon_{ra} = 2.55$, $d_a = 0.02\,\lambda_0$, $\epsilon_{rf} = 12.8$, $d_f = 0.02\,\lambda_0$, $L_p = W_p = 0.29\,\lambda_0$, $L_s = 0.10\,\lambda_0$, $W_s = 0.01\,\lambda_0$, $L = 0.083\,\lambda_0$, $a = b = 0.5\,\lambda_0$.

Fig. 6 shows the reflection coefficient magnitude versus scan angle for a more practical array. The antenna substrate is the same as the previous case, but now the feed substrate is only $0.02\,\lambda_0$ in thickness. This configuration thus simulates an integrated phased array architecture where the antenna elements are on a low dielectric constant substrate, and the feed substrate has a high dielectric constant to model a semiconductor-type material which could be used for active circuitry. Observe that now the blindness associated with the feed substrate has moved out to $\theta = 82.9°$ in the E-plane, due to the thinner feed substrate. The blindness associated with the antenna substrate is still at $\theta = 85.6°$, since this substrate is unchanged from that of Fig. 4. This result shows the feasibility of operating an integrated phased array of aperture coupled patches. Of course, there is still a need for a wide-angle impedance matching technique that could be applied to this array (as well as other printed arrays).

In order to verify the theory, a waveguide simulator using an aperture coupled patch was fabricated and tested. The geometry of this simulator is shown in Fig. 7. The antenna substrate was a rectangle 3.40×7.21 cm, in order to fit into a standard S-band (WR-284) waveguide matched load. The center patch element was aperture coupled to a microstrip feed line on the bottom feed substrate. The "half" patches at the ends of the antenna substrate are not fed, since they are effectively shorted by the waveguide walls. The flange of the waveguide forms a good electrical contact with the ground plane around the antenna substrate, and the waveguide walls image the patches to simulate an aperture coupled patch in an infinite array environment. The feed line and the bottom side of the coupling aperture are not within the waveguide walls, but this should not be a serious problem because the patch element should be radiating the most power. Low dielectric constant material (Duroid 5880, $\epsilon_r = 2.20$) was used for both the antenna and feed substrates to avoid problems with the

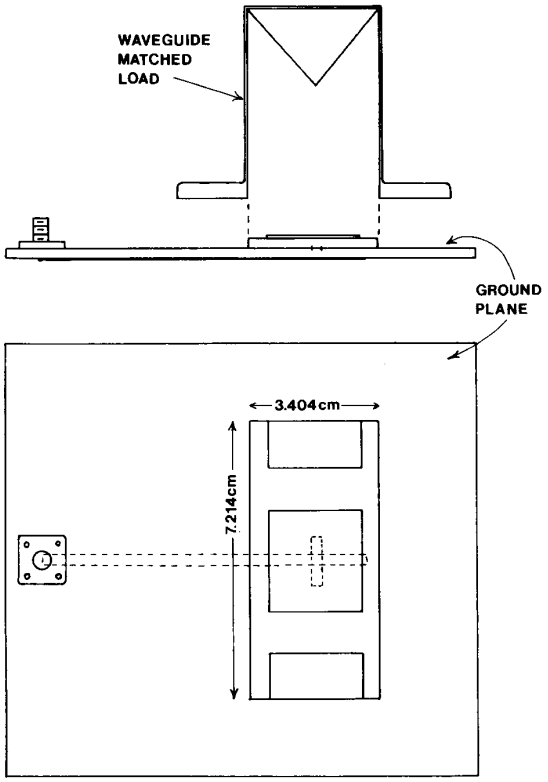

Fig. 7. Geometry of a waveguide simulator using an aperture coupled microstrip patch. $\epsilon_{ra} = \epsilon_{rf} = 2.20$, $d_a = d_f = 0.158$ cm, $L_p = W_p = 2.5$ cm, $L_s = 1.0$ cm, $W_s = 0.1$ cm, $L = 1.3$ cm, $a = 3.404$ cm, $b = 3.607$ cm.

coax-to-microstrip transition, which were noted when a feed substrate with $\epsilon_r = 10.2$ was tried.

The simulator effectively scans in the H-plane to an angle θ, where

$$\sin\theta = \frac{\lambda_0}{4b}, \tag{20}$$

defines the scan angle in terms of the operating frequency.

Fig. 8 shows measured and calculated results for the waveguide simulator of Fig. 7; the phase reference for this data is at the coupling aperture, and the measurements were made with an HP 8510 network analyzer using trace math and a short-circuited reference microstripline. The agreement between measured and calculated results is good.

At the patch resonant frequency at 3.65 GHz, the effective scan angle, from (20), is 34.7°. As the frequency increases from 3.45 GHz to 3.85 GHz, the scan angle decreases from 37.1° to 32.7°.

Also shown in Fig. 8 is the calculated impedance locus for an isolated aperture coupled patch with the same dimensions and substrates as the simulator case. We see an increase of almost 2:1 in resonant impedance compared to the element in an infinite array environment, which leads to further confidence in the present analysis.

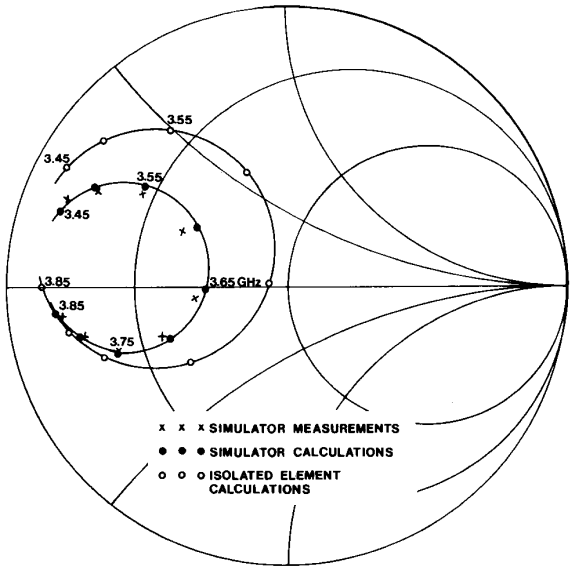

Fig. 8. Calculated and measured results for the waveguide simulator of Fig. 7.

IV. Conclusion

This paper has described an analysis of an infinite array of aperture coupled microstrip patches. Results for reflection coefficient versus scan angle were presented for two cases, and the scan blindness phenomenon was observed and discussed. A notable difference between this geometry and previous printed phased arrays is that, since the aperture coupled patch geometry employs two separate substrates, two distinct scan blindnesses can occur, and can individually be associated with the two substrates.

Measurements from a waveguide simulator were presented, and shown to confirm the theory.

Appendix

The uniform, piecewise-sinusoidal, and entire domain expansion/test mode distributions are

$$f_u(x, W) = \begin{cases} 1/W, & \text{for } |x| < W/2 \\ 0, & \text{otherwise} \end{cases} \tag{21}$$

$$f_p(x, h) = \frac{\sin k_e(h - |x|)}{\sin k_e h}, \qquad \text{for } |x| < h \tag{22}$$

$$f_s(x, k, L) = \sin\frac{k\pi}{L}(x + L/2), \qquad \text{for } |x| < L/2 \tag{23}$$

$$f_c(x, k, L) = \cos\frac{k\pi}{L}(x + L/2), \qquad \text{for } |x| < L/2. \tag{24}$$

Using the following Fourier transform pair,

$$F(k_x) = \int_{-\infty}^{\infty} f(x) e^{-jk_x x}\, dx, \tag{25}$$

$$f(x)=\frac{1}{2\pi}\int_{-\infty}^{\infty}F(k_x)e^{jk_x x}\,dk_x, \tag{26}$$

the Fourier transforms of the above functions can be written as

$$F_u(k_x)=\frac{\sin k_x W/2}{k_x W/2} \tag{27}$$

$$F_p(k_x)=\frac{2k_e\,[\cos k_x h-\cos k_e h]}{\sin k_e h(k_e^2-k_x^2)} \tag{28}$$

$$F_s(k_x)=\left(\frac{k\pi}{2L}\right)\frac{e^{-jk_x L}(-1)^k-e^{jk_x L}}{k_x^2-\left(\frac{k\pi}{2L}\right)^2} \tag{29}$$

$$F_c(k_x)=jk_x\frac{e^{-jk_x L}(-1)^k-e^{jk_x L}}{k_x^2-\left(\frac{k\pi}{2L}\right)^2}. \tag{30}$$

Then the Fourier transforms of the expansion/test mode currents of (4a), (4b) can be written as

$$\bar{F}_i(k_x,\,k_y)=\hat{x}F_s(k_x)F_c(k_y) \tag{31}$$

for $\hat{x}$-directed current modes, and as

$$\bar{F}_i(k_x,\,k_y)=\hat{y}F_c(k_x)F_s(k_y) \tag{32}$$

for $\hat{y}$-directed current modes.

The required Green's function components are listed below in transform domain form:

$$G_{xx}^{EJ}=\frac{-jZ_0}{k_0}\cdot\frac{(\epsilon_r k_0^2-k_x^2)k_2\cos k_1 d+jk_1(k_0^2-k_x^2)\sin k_1 d}{T_e T_m}\cdot\sin k_1 d \tag{33}$$

$$G_{yx}^{EJ}=\frac{jZ_0}{k_0}\frac{k_x k_y\sin k_1 d[k_2\cos k_1 d+jk_1\sin k_1 d]}{T_e T_m} \tag{34}$$

$$G_{xy}^{EJ}=G_{yx}^{EJ}$$

$$G_{yy}^{EJ}=\frac{-jZ_0}{k_0}\cdot\frac{(\epsilon_r k_0^2-k_y^2)k_2\cos k_1 d+jk_1(k_0^2-k_y^2)\sin k_1 d}{T_e T_m}\cdot\sin k_1 d \tag{35}$$

$$G_{xy}^{EM}=\frac{jk_x^2(\epsilon_r-1)\sin k_1 d}{T_e T_m}+\frac{k_1}{T_e} \tag{36}$$

$$G_{yy}^{EM}=\frac{-jk_x k_y(\epsilon_r-1)\sin k_1 d}{T_e T_m} \tag{37}$$

$$G_{yx}^{HJ}=\frac{-jk_x^2(\epsilon_r-1)\sin k_1 d}{T_e T_m}+\frac{k_1}{T_e} \tag{38}$$

$$G_{yy}^{HJ}=\frac{-jk_x k_y(\epsilon_r-1)\sin k_1 d}{T_e T_m} \tag{39}$$

$$G_{yy}^{HM}=\frac{1}{k_0 Z_0}\left[\frac{(\epsilon_r k_0^2-k_y^2)(k_1\cos k_1 d+jk_2\epsilon_r\sin k_1 d)}{k_1 T_m}-\frac{k_1 k_y^2(\epsilon_r-1)}{T_e T_m}\right] \tag{40}$$

where

$$T_m=\epsilon_r k_2\cos k_1 d+jk_1\sin k_1 d, \tag{41}$$

$$T_e=k_1\cos k_1 d+jk_2\sin k_1 d, \tag{42}$$

$$k_1=\sqrt{\epsilon_r k_0^2-\beta^2},\ I_m(k_1)<0, \tag{43}$$

$$k_2=\sqrt{k_0^2-\beta^2},\ I_m(k_2)<0, \tag{44}$$

$$\beta^2=k_x^2+k_y^2, \tag{45}$$

$$k_0=\omega\sqrt{\mu_0\epsilon_0}=2\pi/\lambda_0, \tag{46}$$

$$Z_0=\sqrt{\mu_0/\epsilon_0}. \tag{47}$$

If a two-dimensional Fourier transform pair is defined as

$$G(k_x,\,k_y)=\int_{-\infty}^{\infty}\int g(x,\,y)e^{-jk_x(x-x_0)}e^{-jk_y(y-y_0)}\,dx\,dy, \tag{48}$$

$$g(x,\,y)=\frac{1}{4\pi^2}\int_{-\infty}^{\infty}\int G(k_x,\,k_y)e^{jk_x(x-x_0)}e^{jk_y(y-y_0)}\,dk_x\,dk_y, \tag{49}$$

then the above Green's functions have the following interpretations:

- G_{xx}^{EJ} → E_x at (x, y, d) due to a unit $\hat{x}$ electric current element at (x_0, y_0, d).
- G_{xy}^{EJ} → E_x at (x, y, d) due to a unit $\hat{y}$ electric current element at (x_0, y_0, d).
- G_{yx}^{EJ} → E_y at (x, y, d) due to a unit $\hat{x}$ electric current element at (x_0, y_0, d).
- G_{yy}^{EJ} → E_y at (x, y, d) due to a unit $\hat{y}$ electric current element at (x_0, y_0, d).
- G_{xy}^{EM} → E_x at (x, y, d) due to a unit $\hat{y}$ magnetic current element (or e_x^a slot field) at (x_0, y_0, d).
- G_{yy}^{EM} → E_y at (x, y, d) due to a unit $\hat{y}$ magnetic current element (or e_x^a slot field) at $(x_0, y_0, 0)$.
- G_{yx}^{HJ} → H_y at $(x, y, 0)$ due to a unit $\hat{x}$ electric current element at (x_0, y_0, d).
- G_{yy}^{HJ} → H_y at $(x, y, 0)$ due to a unit $\hat{y}$ electric current element at (x_0, y_0, d).
- G_{yy}^{HM} → H_y at $(x, y, 0)$ due to a unit $\hat{y}$ magnetic current element (or e_x^a slot field) at $(x_0, y_0, 0)$.

ACKNOWLEDGMENT

The author would like to thank Andre Radosh of the University of Massachusetts for fabricating the waveguide simulator element, and Dr. Robert Mailloux of RADC, Hanscom AFB, for pointing out the possibility of scan blindness due to the feed substrate of this type of array.

REFERENCES

[1] D. M. Pozar, "A microstrip antenna aperture coupled to a microstrip line," *Electron. Lett.*, vol. 21, pp. 49-50, Jan. 17, 1985.

[2] D. M. Pozar and D. H. Schaubert, "Comparison of architectures for monolithic phased array antennas," presented at 1985 Phased Arrays Symposium, Boston, MA.

[3] D. M. Pozar, "A monolithic phased array architecture using an aperture coupled microstrip antenna," presented at 1985 IEEE/ Antennas Propagat. Soc. Int. Symp., Vancouver, Canada.

[4] P. L. Sullivan and D. H. Schaubert, "Analysis of an aperture coupled microstrip antenna," *IEEE Trans. Antennas Propagat.*, vol. AP-34, pp. 977-984, Aug. 1986.

[5] D. M. Pozar, "A reciprocity method of analysis for printed slot and slot-coupled microstrip antennas," *IEEE Trans. Antennas Propagat.*, vol. AP-34, pp. 1439-1446, Dec. 1986.

[6] H.-Y. Yang and N. G. Alexopoulos, "Analysis of an aperture coupled dipole antenna, a microstrip fed slot and a slotline fed dipole," in *1987 Int. IEEE Antennas Propagat. Soc. Symp. Dig.*, June 1987, pp. 924-927.

[7] D. M. Pozar and D. H. Schaubert, "Scan blindness in infinite phased arrays of printed dipoles," *IEEE Trans. Antennas Propagat.*, vol. AP-32, pp. 602-610, June 1984.

[8] ——, "Analysis of an infinite array of rectangular microstrip patches with idealized probe feeds," *IEEE Trans. Antennas Propagat.*, vol. AP-32, pp. 1101-1107, Oct. 1984.

[9] A. C. Buck and D. M. Pozar, "An aperture coupled microstrip antenna with a perpendicular feed," *Electron. Lett.*, vol. 22, pp. 125-126, Jan. 30, 1986.

[10] D. M. Pozar and R. W. Jackson, "An aperture coupled microstrip antenna with a proximity feed on a perpendicular substrate," *IEEE Trans. Antennas Propagat.*, vol. AP-35, pp. 728-731, June 1987.

[11] D. M. Pozar, "New architectures for millimeter wave phased array antennas," presented at *JINA* 1986 Int. Symp. Antennas, Nice, France.

[12] ——, "Five novel feeding techniques for microstrip antennas," in *1987 Int. IEEE Antennas Propagat. Soc.*, June 1987, pp. 920-923.

[13] C. C. Liu, A. Hessel, and J. Shmoys, "Performance of probe-fed microstrip-patch element phased arrays," *IEEE Trans. Antennas Propagat.*, vol. 36, pp. 1501-1509, Nov. 1988.

[14] J. T. Aberle and D. M. Pozar, "Analysis of infinite arrays of probe-fed rectangular microstrip patches using a rigorous feed model," *Proc. IEE* (MOA), to be published.

David M. Pozar (S'74-M'80-SM'88), for a photograph and biography please see pages 1349 and 1350 of the December 1987 issue of this TRANSACTIONS.